Compact Nonlinear Model of an Implantable Electrode Array for Spinal Cord Stimulation (SCS)

Jonathan Scott, *Senior Member, IEEE,* and Peter Single

***Abstract*—We describe the construction of a model of the electrode-electrolyte interface and surrounding electrolyte in the case of a platinum-electrode array intended for spinal-cord stimulation (SCS) application. We show that a finite, two-dimensional, resistor array provides a satisfactory model of the bulk electrolyte, and we identify the complexity required of that resistor array. The electrode-electrolyte interface is modelled in a fashion suitable for commonly-available, compact simulators using a nonlinear extension of the model of Franks [4] that incorporates diodes and a memristor. The electrode-electrolyte interface model accounts for the nonlinear current-overpotential characteristic and diffusion-limiting effects. We characterise a commercial, implantable, electrode array, fit the model to it, and show that the model successfully predicts operational characteristics.**

***Index Terms*—Electrical stimulation, Bioelectric phenomena, Biophysics, Bioimpedance, Biomedical electrodes, Biomedical measurements, Implantable biomedical devices**

I. Introduction

THE impedance presented by an electrode in electrolyte is important to the operation of biological implants and a subject of considerable interest in the literature. Merrill et al. give a comprehensive review of the chemistry and characteristics in [1] with the aim of establishing safe limits for therapeutic use in humans. However, the interest is not limited to matters of safety. A large impedance can increase power demand and shorten implant battery life. The reactive nature of the impedance causes pulse tails that cause stimulus-artefact. [2] Operation outside the linear or "small-signal" range can give rise to obscuring signal artefacts, present on sensing electrodes, that cannot readily be removed by blanking and subtraction. [3]

Franks et al. have presented a model of the electrode-electrolyte interface that is valid for small variations of the potential drop across the interface. [4] Such variations in the half-cell voltage are referred to as the overpotential. The model consists of a small spreading resistance in series with the parallel combination of two elements. The first of these elements is a so-called Constant Phase Element (C.P.E. or CPE), otherwise known as a fractional-pole capacitor. [5] It represents the charge-transfer contribution of ionic species in the Helmholtz layer adjacent to the metallic surface of the electrode. The second parallel element is approximated as a resistor. In the model of [4] this resistor represents the Faradaic reactions that take place at the electrode interface. The approximation is valid only for overpotentials in the millivolt range, and for short durations. Electronics Engineers refer to models that contain such approximations as "small-signal models". They are extremely useful for simplifying circuit calculations, but are not valid for larger excursions.

In neuromodulation for Spinal Cord Stimulation (SCS) relatively large amounts of charge flow through the implanted electrodes. This is necessary to recruit neurones in the spinal cord, as the electrode array is normally placed in the epidural space, outside the dura, and several millimetres may separate the electrode array and the target neurones. This manuscript proposes a medium-signal electrode model that incorporates the reversible nonlinear processes that occur when the overpotential is no longer held small. [6] We reserve the term "large signal" for operation outside the so-called "water window" where irreversible reactions, such as electrolysis, occur.

II. Bulk Electrolyte Model

In this manuscript a model will be fitted to a commercial SCS electrode array in 1/10 phosphate-buffered saline (PBS). The selected array is an Octrode from St Jude Medical. [7] This electrode array consists of a cylindrical assembly approximately 1mm in diameter with alternating conducting and insulating spacer bands. The 8 conducting electrodes are platinum cylindrical sections spaced 7mm apart, each 3mm long and having a geometrical area of approximately 10 square mm and an electrical area of approximately 14 square mm, owing to surface roughness. Inter-electrode capacitance is in the region of a few tens of picofarads for adjacent electrodes, varying with the details of the connection electronics. The 1/10 phosphate-buffered saline has been used as it is a reasonable approximation to the combination of cerebrospinal fluid, bone, nervous tissue, etc., in which SCS arrays normally operate in vivo, and is repeatable.

Figure 1 depicts a section of the electrode array and a set of resistors to represent the electrolyte. We propose to model the bulk electrolyte as a 2-dimensional array of resistors, owing to the rotational symmetry. Consider the cylindrical array to be surrounded by a series of annular zones. Each zone extends from a radius r_i to a larger radius r_{i+1}, starting at the boundary of the electrode. The resistance values can be estimated by finding the radial and longitudinal resistances

Jonathan Scott is with the School of Electronic Engineering, University of Waikato, New Zealand, e-mail: (jonathanscott@ieee.org).

Peter Single is with the Implant Technology Group, NICTA, and Saluda Medical, Redfern, Sydney.

Manuscript received 2013.

of annular sections. A radial resistor associated with the electrolyte surrounding an electrode section will take on the value determined by computing the resistance between the inner and outer cylindrical walls of the annular cylinder of electrolyte. Similarly for radial resistors corresponding to insulating sections. These electrode and spacer radial resistances will differ if the electrodes and insulators are of unequal length, as in our case. The longitudinal resistors take the value found for the resistance between the upper and lower annular surfaces of the notional sections of radii r_i and r_{i+1} and whose height is half the sum of the heights of an electrode and an insulating segment. Taking a series of annular rings whose radial thickness doubles with each step outward, $\frac{r_{i+1}}{r_i} = 2$. The resistivity, ρ, of 1/10 PBS is about 11620Ωmm, $l_e = 3$mm, $l_s = 4$mm. Some algebra proves that

$$R_{eri} = \frac{\rho}{2\pi l_e} \ln \frac{r_{i+1}}{r_i} \approx 427\Omega \tag{1}$$

$$R_{sri} = \frac{\rho}{2\pi l_s} \ln \frac{r_{i+1}}{r_i} \approx 321\Omega \tag{2}$$

and

$$R_{li} = \rho \frac{l_e + l_s}{2} / \left[\pi \left(r_{i+1}^2 - r_i^2\right)\right] = \frac{\rho}{2\pi} \frac{l_e + l_s}{r_{i+1}^2 - r_i^2} \tag{3}$$

where R_{eri} is the resistance corresponding to the i^{th} layer surrounding an electrode in the radial direction, R_{sri} is the resistance corresponding to the i^{th} layer surrounding an insulating spacer in the radial direction, R_{li} is the longitudinal resistance between the centrelines of an electrode and a spacer, l_e is the longitudinal length of an electrode, and l_s is the longitudinal length of an insulating spacer. Note that all the radial resistors will have the same values, while the longitudinal resistors will reduce in value by a factor of four for each step outward.[1] The commencing value for our dimensions is 1100Ω, descending to 275Ω, 69Ω, etc. After some number of meshes, the network is terminated in a star network representing the saline bath "at infinity".

Figure 2 depicts the topology proposed to model the bulk electrolyte in which the electrode resides. The mesh of resistors model the electrolyte, taking on values in accordance with the calculations above. Previous models of the bulk electrolyte have represented it with a single-layer ladder network. [3]

We suggest two experiments to provide data against which predictions of the model can be tested. Each consists of driving one electrode of the array with a current and using a second electrode for the return current. The voltage dropped across the (potentially nonlinear) interface region is not known. However, voltages measured between pairs of the six other electrodes can be used. If a suitably high-impedance voltage measurement instrument is used, the ac voltage between the metal electrodes may be assumed to be equal to the ac voltage between points in the electrolyte immediately adjacent to the electrodes; this is the case because a negligible ac voltage will be dropped across the interface branch. It is possible to measure the voltage between pairs of electrodes, other than the two carrying the stimulus current, and obtain the transresistance. If the current is fed into electrode 1 and returned through electrode 8, the five voltages $V_{i,j}^{1,8}$ for

[1]The factor of 4 reduction with each step is a consequence of our choice to consider annular sections whose radial dimensions double each step outward. Other choices are possible. Note that our choice leads to a resistor array having constant radial but geometrically varying longitudinal resistances.

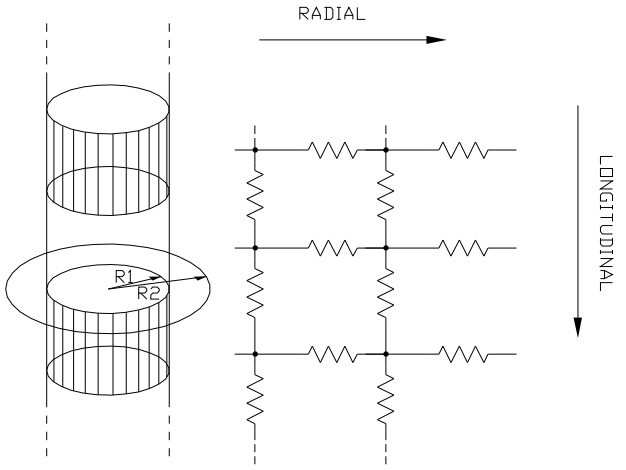

Fig. 1. Geometry of a section of the cylindrical electrode array showing two electrodes (shaded) and an insulating segment with a snippet of the resistor mesh to be derived from the conducting electrolyte that surrounds the electrode array.

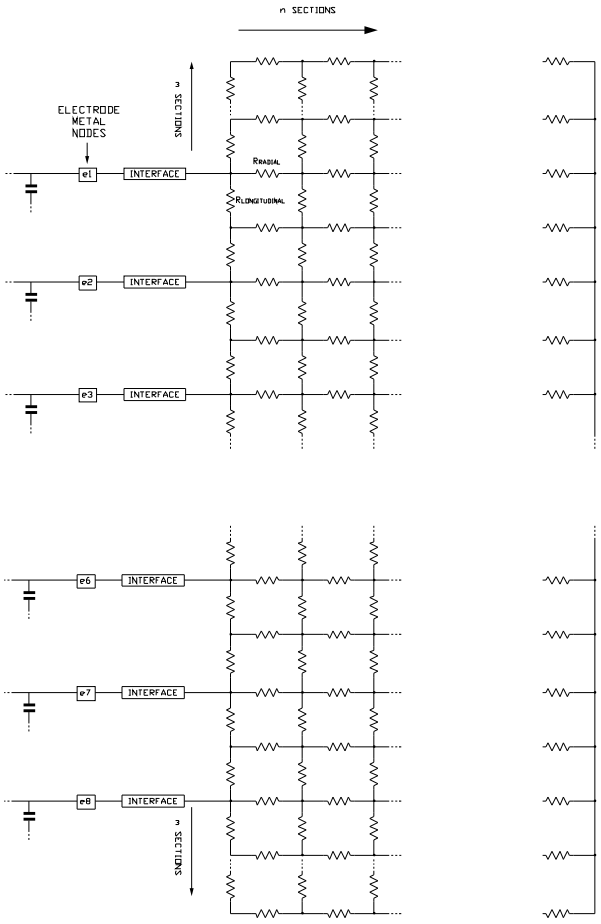

Fig. 2. Schematic of the model of the 8-electrode array in electrolyte. The interface properties are modelled by the branches marked "interface".

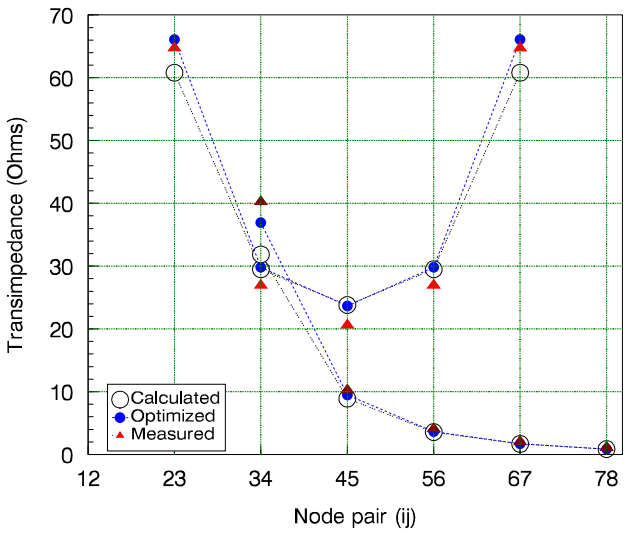

Fig. 3. Measured and simulated transimpedances of the bulk electrolyte. Measured data are represented by triangles, simulated data by circles or dots. The circles are values derived from resistances calculated from physical considerations, the dots from values after optimisation. The parabolic group are measured with signal current applied on electrode 1 and current returned via electrode 8, the hyperbolic group with current applied on electrode 1 and current returned via electrode 2. The x-axis identifies the pair of electrodes across which voltage is measured, the y-axis the measured voltage divided by the current flowing in electrode 1.

$2 \leq i,j \leq 7$ and $i \neq j$ yield five transresistances of the form $R_{ij}^{1,8} = V_{i,j}^{1,8}/I_1$. Similarly, if the current is fed into electrode 1 and returned through electrode 2, the five transresistances $R_{ij}^{1,2} = V_{i,j}^{1,2}/I_1$ for $3 \leq i,j \leq 8$ and $i \neq j$ are obtained. These 10 values have been measured for our electrode array in 1/10 PBS.[2] The measurements were carried out using a TPS2014B oscilloscope with 10MΩ input resistance and 20pF input capacitance at a frequency of 10Hz for a current of 3mA peak. Current and voltage signals remained undistorted and in phase for all measurements, confirming that the saline produces resistive impedances. The measured data are plotted in figure 3. The figure also presents values simulated using the calculated resistance parameter values presented above, and after the three resistance values are manually trimmed to improve the fit. The agreement is remarkably good for the directly-calculated values, suggesting that the approach is sound. The fit can be slightly improved, presumably compensating for errors arising from the discrete nature of the approximation. Experiments suggest that a mesh 5 layers deep and with 3 layers on each edge is more than sufficiently detailed: Increasing these has no impact on the numerical results, decreasing them had no significant impact on simulation speed.

III. The Electrode-Electrolyte Interface

As noted above, two mechanisms occur to facilitate current flow across an electrode-electrolyte interface. One mechanism is a 'displacement' current flow in the so-called Helmholtz layer, a double-layer of charge. The displacement current corresponds to the time-derivative of electric displacement field term in Maxwell's current equation. This capacitor-like phenomenon is often modelled as a pure electrical capacitance, often called the 'double layer capacitance'. [4], [6] More accurately it is described as a Constant Phase Element or more rigorously as a fractional-pole element. [5]

The second mechanism is associated with movement of charged species in the electrolyte and exchange of charge across the boundary between electrode and electrolyte. This is termed a 'Faradaic' current. When very small it can be modelled as a simple resistor. [4] The task now is to translate these descriptions into an electrical equivalent circuit that can be entered into compact simulators.

A. The Displacement Part

Fractional-pole capacitors are not supported in time-domain compact circuit simulators such as the ubiquitous SPICE, since a non-integral power of the complex frequency variable s corresponds to an infinite sum of exponentials in the time domain.[3] A number of methods of representation have been investigated, as their importance in both pure electronic and biological systems was recognised many decades ago. [13] Although not particularly efficient either to enter or compute, this work will use a lumped-RC approximation, suitable for direct implementation in compact circuit simulators, attributed to Morrison. [14] Each constant-phase element (CPE) is replaced with a set of series-RC branches in parallel. The circuit appears in figure 4. The number of branches is theoretically infinite, but given a required phase tolerance and a finite frequency range over which the approximation must hold, Morrison has done the very considerable amount of "tedious algebra" to provide equations that yield the number of branches and the values of the resistor and capacitor in each branch. These equations are readily evaluated in a script that produces a subcircuit suitable for inclusion in a circuit simulator.

From [14],

$$|Y'_\theta| \approx \frac{(wRC)^{\frac{1}{m}}}{R} y_\theta \tag{4}$$

where $|Y'_\theta|$ is the magnitude of the approximation Y'_θ to the CPE admittance Y_θ, R and C are the values of resistance

[2]There are actually only 8 independent data gathered in these experiments since of course, $V_{i,j}^{p,q}$ and $V_{j,i}^{p,q}$ are the same voltage, and symmetry requires that $V_{3,4}^{1,8} = V_{5,6}^{1,8}$ and $V_{2,3}^{1,8} = V_{6,7}^{1,8}$.

[3]The vast majority of computer simulation of electrical circuits is carried out using a program called SPICE. [9] Throughout much of the 1980s and 1990s proprietary versions called 'HSPICE' and 'PSPICE' dominated the industry. Dozens of textbooks appeared to help students use PSPICE, for example see [10] and [11]. Today SPICE is available free of charge on all common platforms. All versions support a common kernel of input and output formats, and all versions work similarly. The method is essentially nodal analysis with iterative numerical solution of the first-order differential equations that yields node voltages and branch currents as a function of time. Thus SPICE is limited to impedances and transimpedances whose constitutive relationships can be expressed with finite equations relating instantaneous voltage, current and their derivatives. As such, it is not readily able to incorporate fractional-order elements. There exists another type of simulator that employs the "harmonic balance" (HB) technique, substantially through the work of Kundert. [12] Rather than solving Kirchoff's equations at discrete points in time, the HB solver operates in the frequency domain, and achieves an energy balance considering periodic signals at a finite, predefined set of frequencies. It is possible to represent fractional-order elements in HB simulators. However, simulators with an HB solver such as Agilent's ADS and AWR's Microwave Office are tailored for the RF community, and are not free.

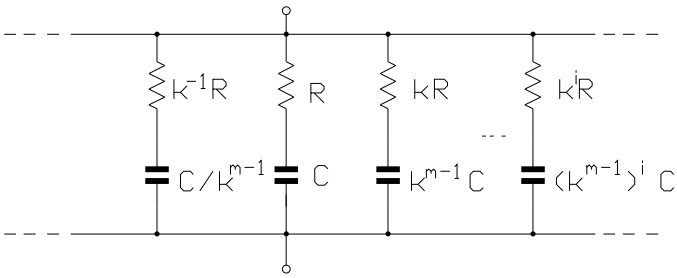

Fig. 4. Infinite-RC-series model of a constant-phase element, after [14]. The counter i ranges such that the time constant τ of the first and last branch span the required bandwidth. The parameter k is chosen to set the "density" of branches which is related to the accuracy of the approximation.

and capacitance in the equivalent circuit of figure 4, ω is the radian angular frequency as usual, $1 \leq m \leq \infty$ is a parameter reflecting the value of the constant phase of the element, and

$$y_\theta = \frac{\pi}{m \ln k} \sec \frac{1}{2}\pi \left(1 - \frac{2}{m}\right) \tag{5}$$

where $k > 1$ is a parameter controlling the multiplicity or "density" of branches with respect to frequency, in the equivalent circuit[4]; also

$$\angle Y'_\theta \approx \frac{\pi}{2m} - \theta_p \sin \left[\frac{2\pi \ln \omega RC}{m \ln k} - \frac{1}{2}\pi \left(1 - \frac{2}{m}\right)\right] \tag{6}$$

where $\angle Y'_\theta$ is the argument of the approximation Y'_θ, and

$$\theta_p \approx \frac{m \ln k}{\pi} \frac{\cosh \frac{\pi^2}{m \ln k}}{\cosh \frac{2\pi^2}{m \ln k}} \cos \frac{1}{2}\pi \left(1 - \frac{2}{m}\right). \tag{7}$$

Note that y_θ given by (5) and θ_p given by (7) are purely functions of m, k, and natural constants. Equation (4) provides the magnitude of the admittance of the CPE with a scaling factor provided by equation (5), while equation (6) provides the phase of the CPE including a periodic error governed by equation (7). The problem of modelling the displacement component now reduces to finding values of m, k, R, C, and the multiplicity of branches in the equivalent circuit in order to generate a lumped subcircuit to approximate the CPE in an electrode model over a specified frequency range. Measurements of impedance phase angle and impedance magnitude as a function of frequency constitute the measured data by means of which the fitting may be executed.

Looking at (6) the first term provides the substantive relationship between the constant phase and the parameter m so that one may determine m using

$$m = \frac{\pi}{2\theta_{CPE}} \tag{8}$$

where θ_{CPE} is the constant phase value determined from measurement. Thence equations (6) and (7) above provide a means to relate a required phase accuracy of the approximation to the multiplicity factor k. Rather than trying to relate phase accuracy to simulation accuracy, it proves easier simply to make k sufficiently close to 1 that simulation results do not change; in other words we will simply reduce k "far enough" towards 1. Given values for m and k, a measure of $|Y_\theta|$ at a frequency $\omega = \omega_0$ permits determination of one pair of values for R and C using equation (4). Finally the number of branches is determined given the bandwidth over which the network is expected to operate by suitable truncation of the infinite series of RC pairs. In the case of SCS this is typically 10–10,000 Hz or less, often 40–2,000 Hz.

[4]Morrison's parameter k should not be confused with Boltzmann's constant k that appears in the discussion of Faradaic effects.

B. The Faradaic Part

The best available theory for the Faradaic current across the boundary describes it by the more general form of the Butler-Volmer equation, sometimes called the current-overpotential equation: [1]

$$i_{\text{net}} = i_0 \left\{ \frac{[O]_{(0,t)}}{[O]_\infty} e^{-\alpha_c n f \eta} - \frac{[R]_{(0,t)}}{[R]_\infty} e^{(1-\alpha_c) n f \eta} \right\} \tag{9}$$

where i_{net} is the net Faradaic current across the interface, i_0 is the exchange current density, $[O]_{(0,t)}$ and $[R]_{(0,t)}$ are the concentrations of oxidising species and reducing species at the electrode surface ($x = 0$) as functions of time, $[O]_\infty$ and $[R]_\infty$ are the bulk concentrations of oxidising species and reducing species in the electrolyte, $\alpha_c \approx \frac{1}{2}$ is the cathodic transfer coefficient, n is as usual the number of moles of electrons per mole of reactant oxidised, $f \triangleq \frac{F}{RT}$ where $F \approx 96,485$ is Faraday's constant, $R \approx 8.314$ is the gas constant, T is the absolute temperature, and η is the overpotential. It should be noted that this equation is associated with a single given oxidation reaction. Several candidates are identified in [1], and in general there might be multiple similar terms of the form of the right-side of (9) if multiple species are involved simultaneously.

It has been observed before that there is a resemblance between each exponential term of this equation and the diode equation: [6]

$$i_{\text{D}} = I_S \left(e^{\frac{V_D}{n_I V_T}} - 1 \right) \approx I_S e^{\frac{V_D}{n_I V_T}} \tag{10}$$

where i_D is the diode current, V_D is the voltage drop across the diode junction, I_S is the saturation current, $n_I \approx 1$ is the ideality factor[5], and $V_T \triangleq \frac{kT}{q}$ where $k \approx 1.38 \times 10^{-23}$ is Boltzmann's constant, T is the absolute temperature, and $q \approx 1.60 \times 10^{-19}$ is the charge on the electron. Since the charge of a mole of electrons, qN_A, is Faraday's constant, F, and the gas constant, R, is the product of Avogadro's number and Boltzmann's constant, $N_A k$,

$$\frac{F}{R} = \frac{q}{k} \tag{11}$$

and it becomes straightforward to break out each term in equation (9) in the form of the diode equation. The saturation current is replaced by the concentration terms multiplied by the exchange current density, so that

$$I_{S_O} :\sim i_0 \frac{[O]_{(0,t)}}{[O]_\infty} \tag{12}$$

[5]The usual symbol for the ideality factor in equation (10) is simply n, but in order to avoid confusion with the ratio of moles of electrons to moles of reactant in equation (9) the symbol n_I will be used herein.

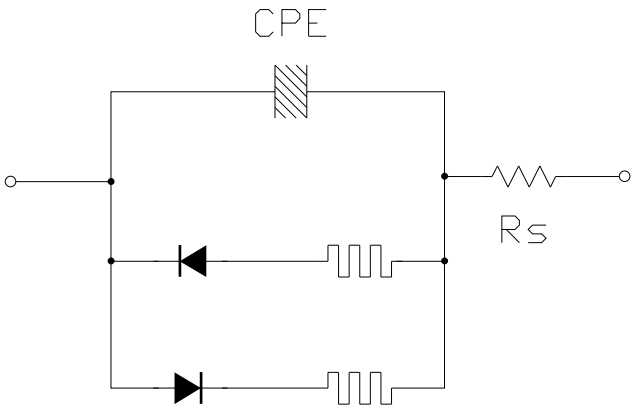

Fig. 5. Proposed model of the electrode-electrolyte interface, containing a constant-phase element, two diodes, two memristors, and a series resistance.

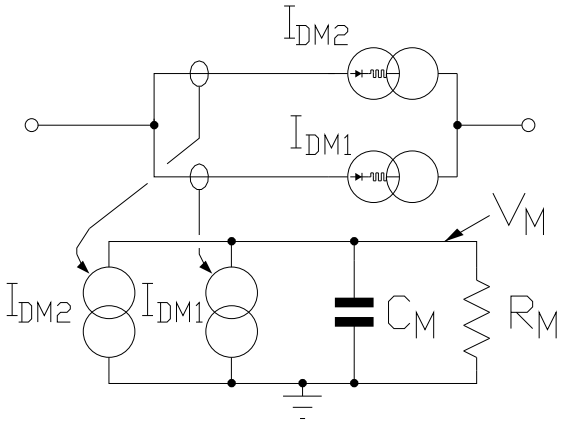

Fig. 6. The subcircuit used to implement the diode-memristor branches. I_{DM1} and I_{DM2} represent the two terms of equation (14), evaluated using (16) and (17). Charge conducted through the two diode-memristor branches is accumulated in capacitor C_M, giving rise to voltage V_M that is subsequently used to calculate I_{DM1} and I_{DM2}.

and

$$I_{S_R} \coloneqq\sim i_0 \frac{[R]_{(0,t)}}{[R]_\infty} \tag{13}$$

where the sub-subscripts O and R refer to the oxidation and reduction parts of the equation.

Now we may rewrite equation (9) as

$$i_{\text{net}} = I_{S_O} e^{\left(\frac{\eta}{n_O V_T}\right)} - I_{S_R} e^{\left(\frac{\eta}{n_R V_T}\right)} \tag{14}$$

where the ideality constants $n_O = \frac{1}{n\alpha_c}$ and $n_R = \frac{1}{n(1-\alpha_c)}$, and η has its sign changed on one half to allow for the reverse orientation of the second diode. This equation corresponds to a circuit consisting of a pair of back-to-back diodes. Close to equilibrium, where the concentrations of species at the electrode surface equal those in the bulk electrolyte $I_{S_R} = I_{S_O} = i_0$.

As eloquently explained by Merrill et al., the concentration of species at the electrode surface will decline as the net transferred charge increases. [1] This will have the effect of reducing the current conducted in response to the amount of charge transferred. This characteristic—variation of conductance with the sum of charge conducted—is that of a memristor. [8] We now postulate an extension of the linear model, drawn in figure 5. R_S is the ohmic spreading resistance and is expected to be in the order of R_{eri}. The CPE represents the double layer as in the model of Franks et al., to be discussed in more detail below. The Faradaic pathway comprises the two diodes with their associated memristors. Note that this model ignores the dc contribution of the half-cell potential, $\Delta\phi$, as this is of no interest in our situation. [1]

One complication arises, in that the accumulated charge associated with the two memristors is "shared". The shared memristor charge can be understood by considering the chemistry at work. For Pt electrodes, hydrogen atom plating and oxide formation and reduction are possible reversible reactions (refer [1], equations 1.4 and 1.6). Consider the plating reaction:

$$Pt + H^+ + e^- \longleftrightarrow \text{Pt—H} \tag{15}$$

As the reaction goes to the right H^+ is consumed, and Pt—H produced, and vice versa. The concentrations $[O]_{(0,t)}$ and $[R]_{(0,t)}$ are constrained for t small, such that one rises as the other falls, since their sum is fixed. In other words, the model must track the charge transferred through the pair of branches representing the Faradaic contribution, and adjust the diode conduction accordingly.

As elements with a dependence upon accumulated charge are not natively supported in any contemporary circuit simulators, the memristor-diode branches will be modelled using current-controlled current sources. Figure 6 depicts the subcircuit that implements the macromodel. The capacitor C_M accumulates the charge transferred through both branches, and is the memory of the memristors. Since $Q = CV$, the voltage V_M becomes the control variable for the memristor characteristic with $V_M = 0$ at equilibrium. The two halves of equation (14) are implemented using

$$I_{S_O} = i_0(1 - V_M) \tag{16}$$

and

$$I_{S_R} = i_0(1 + V_M) \tag{17}$$

with V_M ranging $-1 \leq V_M \leq +1$ where the extrema ± 1 represent the complete depletion of oxidating and reducing species at the electrode surface. The capacitor C_M is then the scaling factor selected to fit the model to the physical dimensions, species concentrations, etc. The parallel resistor R_M introduces a time constant for the diffusion of species towards equilibrium.

C. Model Fitting

The aim in this section is to describe a sequence of measurements and calculations that lead to a set of model parameters and that are readily automated or repeated. Measurements for frequencies above 5Hz have been made with an HP4192A vector impedance meter. At lower frequencies a Tektronix TPS2014B oscilloscope and an Agilent 33220A arbitrary function generator were used. All instruments were controlled via an E5810A GPIB interface with software written in C, Python, AWK, etc.

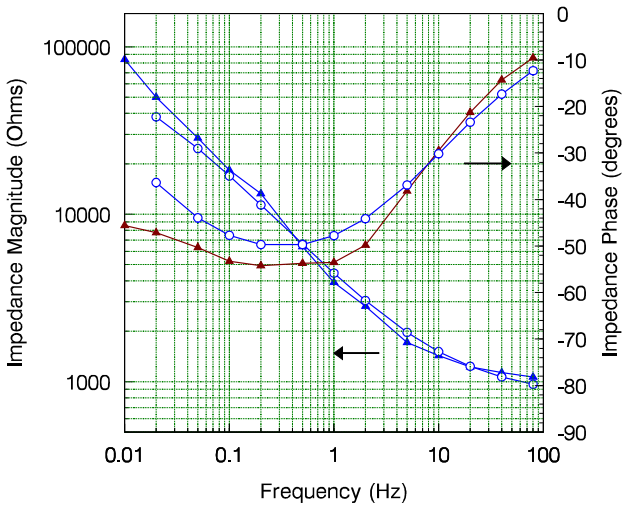

Fig. 7. Magnitude and phase versus frequency of the small-signal impedance from stimulated electrode to an adjacent electrode, representing electrode impedance plus a small contribution from the resistor grid. Measured data is marked with triangles, simulated data with circles.

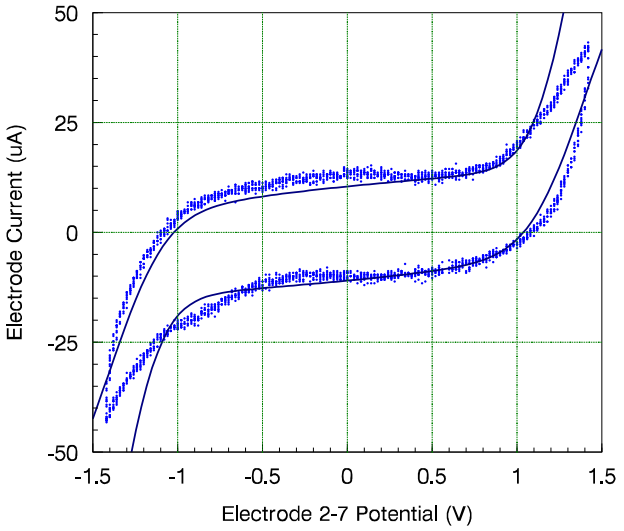

Fig. 8. Voltage across versus current through an electrode pair stimulated with a medium-signal, 20mHz, triangle wave. Symbols are measured data, the continuous line is simulated data.

1) Displacement Branch Parameters: Consider the measurements presented in figure 7. The impedance plotted was calculated by measuring the current injected into electrode 2 and returned via electrode 7, and dividing that into the voltage measured between electrode 7 and electrode 6. We used 2 and 7 to avoid end effects. The voltage on electrode 6 will be close to the voltage at the solution side of electrode 7, but results in an impedance that is increased by a small resistance contributed by the saline, represented by the resistor grid previously determined.

For small currents and adequately large frequencies, virtually all current through an electrode is carried by the CPE branch because its impedance is relatively low and the voltage across the CPE is small enough for the Faradaic branch to hardly conduct at all. We expect the value greater than R_S to be found for higher frequencies, where $X_{CPE} \to 0$. The characteristics of the CPE will dominate for lower frequencies as $X_{CPE} \gg R_S$. It is observed that $R_S \leq 950\Omega$ from the asymptotic behaviour above 1 kHz. The exact value of R_S is found by comparison of simulated values with measured values for frequencies above 1 kHz, by adjusting the value fed into a SPICE simulation until the results agree. For our electrode $R_S = 504\Omega$. As expected, the value is slightly larger than R_{eri}.

At frequencies below 1Hz, X_{CPE} dominates and R_S can be ignored. Unfortunately, in order for the signal to remain small enough for the Faradaic contribution to be negligible, the stimulus current must be kept quite small and noise affects measurement accuracy, so there is a tradeoff. We used increasing time-domain averaging and Fourier processing to recover data as frequency dropped. The phase data in the plot becomes uncertain faster than the magnitude, and it is wiser to extract the CPE angle from the slope of the magnitude-frequency plot in the region where this describes a straight line on log-log scales, $0.01 \leq f \leq 1$Hz, where $\omega = 2\pi f$. So

$$\theta_{CPE} = \frac{\pi}{2}\frac{\Delta\log(Z)}{\Delta\log(f)} \approx 60^o \tag{18}$$

Using (8)

$$m = \frac{\Delta\log(f)}{\Delta\log(Z)} \approx 1.50 \tag{19}$$

and from (5)

$$y_\theta \approx \frac{\pi}{1.50\ln k} \tag{20}$$

At this point a value is guessed for k. We have used $k = 1.2$. Phase deviation was only visible for values above $k \approx 1.8$, but the computational cost of the lower value was negligible. Next, equation (4) leads to a relationship between R and C. One of these may be chosen arbitrarily and the other is found using a $|Y_\theta|$ value on the line of best fit to the region where θ_{CPE} dominates. This leads to the infinite sequence of values as depicted in figure 4. The series is then truncated by incorporating only the RC pairs whose time constants fall within or close to the bandwidth to be covered by the model. For operational simulations we will use the range $10 \leq f \leq 10,000$Hz, but for purposes of comparison with measured values used to fit the model this range is extended to $0.001 \leq f \leq 100,000$Hz, again because it is computationally easy to do so.

2) Faradaic Branch Parameters: The Faradaic model requires values for three parameters, i_0, C_M, and R_M.

Figure 8 plots current against voltage across electrodes 2 and 7 with a triangle-wave stimulus. A triangle wave is used because it allows the contributions of the displacement and Faradaic branches to be separated easily: The observed hysteresis is a result of the square-wave-shaped current that flows in the CPE, while the exponential current characteristic results from the diodes turning on, one in each of the two electrode interfaces. The simulated data plotted in the figure has the memristor functions disabled in order to allow the i_0

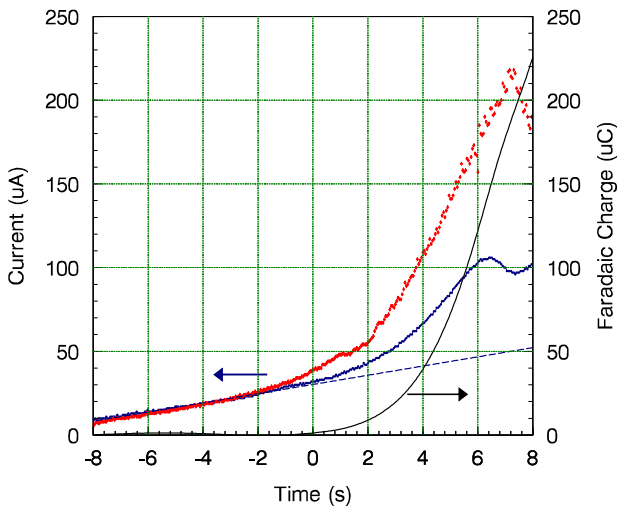

Fig. 9. Current conducted through an electrode pair in still PBS subjected to a ramp voltage stimulus (solid joined dots) is plotted along with the same in agitated solution (scattered symbols). Also shown is the linear extrapolation of the portion before the diodes turn on (dashed line). Finally the net Faradaic charge conducted through the diode-memristor combination (solid line).

parameter to be fitted first. A value of $i_0 \approx 500$pA for an $n = 1$ process, such as hydrogen plating, produces the best agreement at the first onset of the exponential characteristic.

Next we turn to figure 9 that plots current and charge conducted against time in response to a similar ramp voltage stimulus. The onset of diode conduction is visible as before up to a point, beyond which the current starts to fall, in response to the depletion of the species being reduced in one electrode and oxidised in the other. At this point it is tempting to determine a value for C_M off the charge axis of the plot, but it turns out for 1/10 PBS that so low a frequency is required to reveal the Faradaic current above the displacement current that diffusion processes compete in the measurement, and values of C_M and R_M must be selected together. It is clear that a good starting value for C_M will be in the order of a few hundred μF, and R_M will be in the order required to conduct 100μA for a potential of 1V, or about 10kΩ. Manual optimisation is all that is required to achieve reasonable agreement between measurement and simulation as shown in figure 10. The final values are $R_M \approx 15$kΩ and $C_M \approx 200\mu$F.

It is worth noting that the memristor's effect is highly dependent upon the physical supply of species. This is starkly demonstrated by comparison of the still-fluid measurement with a parallel measurement taken while the saline bath is mixed, shown as the scattered-point trace in figure 9. It is also interesting to note the up-turn of the current-voltage characteristic visible in measured data traces in figures 9 and 10. We attribute this to the onset of another diffusion-choked diode characteristic. We have chosen not to pursue this as it should never come into play in normal operation of SCS systems. However, there would seem to be no reason in principle why further diode-memristor branches should not be included in the model to address reactions that commence at higher interface voltages. Typical model parameters for our implantable electrode array are summarised in table I.

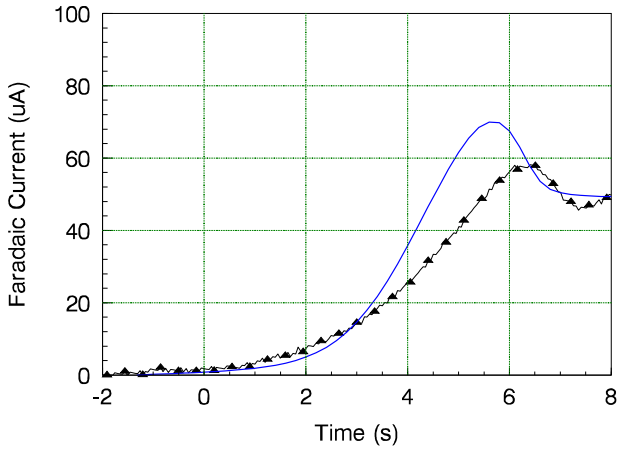

Fig. 10. An estimate of measured Faradaic current conducted through an electrode pair in still PBS subjected to a ramp voltage stimulus, along with the simulated value. Measured data is marked with triangle symbols.

Parameter	Value	Units
R_{eri}	430	Ω
R_{sri}	320	Ω
R_{li}	1100	Ω
R_S	504	Ω
mesh depth	5	# layers
edge depth	3	# layers
m	1.5	
k	1.2	
$\omega/\|Z\|$	0.63/18300	rad/sec & Ω
i_0	500×10^{-12}	Amperes
C_M	200×10^{-6}	Farads
R_M	15,000	Ω

TABLE I
MODEL PARAMETER VALUES.

IV. Model Verification

The most rigorous test of a model is to predict measurements quite separate from those used to fit the parameters. Figure 11 shows measurements and simulations with a 4mA biphasic pulse, typical of SCS therapy. The pulse was applied to electrode 2 of an Octrode with electrode 7 grounded. There is good agreement between simulated and measured data.

At the other extreme of subtlety, figure 12 presents the plot of dc current that is induced when a well-matched biphasic pulse of 6mA peak amplitude is applied to electrodes in 1/10 PBS. The measurements are made by means of a 100kΩ resistor in parallel with a 100μF capacitor, both in series with the generator. This measurement confirms that the model is able to predict nonoampere rectified currents that arise as a result of the Faradaic characteristics of the electrode subjected to microsecond-duration, milliampere-sized, current pulses with 100Hz pulse repetition frequency (PRF). We consider this to be a significant indicator of the value of the model, allowing confirmation that a stimulus regime will remain within patient safety limits before it is physically tested or indeed before any prospective hardware has been constructed.

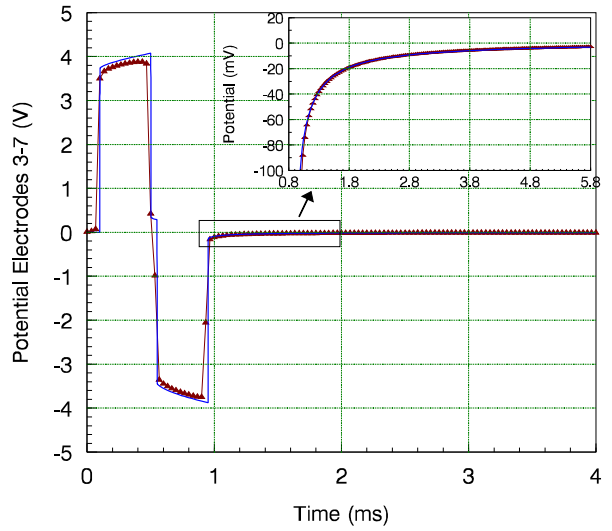

Fig. 11. Measured and simulated voltage between electrode 3 and ground, with electrode 7 grounded and a 4mA biphasic stimulus pulse applied to electrode 2. The inset magnifies the artefact at the tail of the last stimulus pulse. The measured data points exhibit a slewing phenomenon whose effect upon pulse edges should be disregarded; it arises in the 24-bit digitiser that has a maximum sample rate of 30kHz and a $\approx 30\mu$s aperture and so fails to capture the pulse edges faithfully.

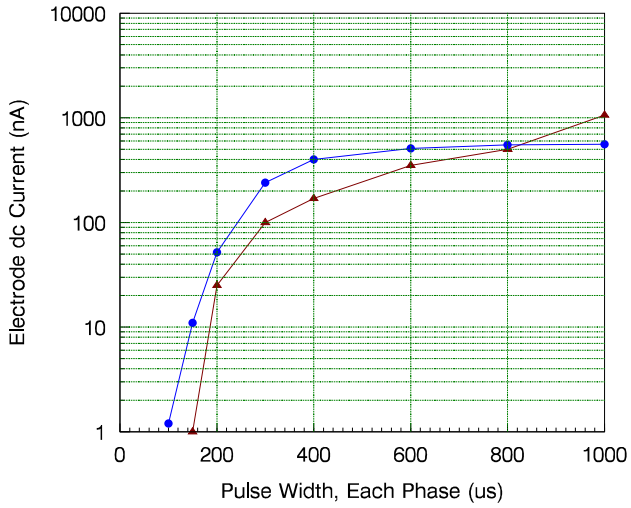

Fig. 12. Measured (triangles) and simulated dc current that flows when a 6mA biphasic pair of pulses with 50μs spacing and varying width are applied between electrodes 2 and 7 on an Octrode.

V. Conclusion

We present a nonlinear model for an electrode in saline electrolyte that is suitable for use in the common electrical simulator. We have fitted that model to an electrode intended for human implantation. We verify the accuracy of the model by prediction of characteristics different from those used to fit the model, and that are representative of signals present in pain relief application of Spinal Cord Stimulation. This model can provide insight into the operation of implanted systems that is not available by any other means.

References

[1] Daniel R. Merrill, Maron Bikson and John G. R. Jefferys, "Electrical stimulation of excitable tissue: design of efficacious and safe protocols", Journal of Neuroscience Methods 141 (2005), pp171–198.
[2] Edgar A. Brown, James D. Ross, Richard A. Blum, Nam Yoonkey, Bruce C. Wheeler, and Stephen P. DeWeerth, "Stimulus-Artifact Elimination in a Multi-Electrode System", IEEE Trans. Biomedical Circuits and Systems, Vol. 2, no. 1, 2008, pp10–21.
[3] US Patent 0244410 A1, "Removing artefact in evoked compound action potential recordings in neural stimulators", Gene Fridman and Rankiri Karunasiri, October 18, 2007.
[4] W. Franks, Iwan Schenker, Patrik Schmutz, and Andreas Hierlemann, "Impedance Characterization and Modeling of Electrodes for Biomedical Applications", *IEEE Transactions on Biomedical Engineering*, vol. 52 no. 7, July 2005, pp1295–1302.
[5] Ahmed S. Elwakil, "Franctional-Order Circuits and Systems: An Emerging Interdisciplinary Research Area" IEEE Circuits and Systems Magazine, Fourth quarter, 2010, pp40–50.
[6] E. T. McAdams, A. Lackermeier, J. A. McLaughlin, and D. Macken, "The linear and non-linear electrical properties of the electrode-electrolyte interface", *Biosensors & Bioelectronics*, vol. 10, 1995, pp67–74.
[7] St. Jude Medical, Octrode Percutaneous Lead for Neuromodulation, http://www.sjmneuropro.com/Products/US/Percutaneous-Leads.aspx, retrieved December 2012.
[8] L. Chua, "Memristor—The Missing Circuit Element", IEEE Transactions on Circuit Theory, vol. CT-18, no. 5, September 1971, pp507–519.
[9] L. W. Nagel, "The 40^{th} Anniversary of SPICE: An IEEE Milestone", *IEEE Solid-State Circuits Magazine*, Vol. 3, no. 2, 2011. (The issue contains numerous articles about the history of SPICE.)
[10] P. W. Tuinenga, *SPICE: A Guide to Circuit Simulation and Analysis using PSPICE*, Prentice–Hall, 1988.
[11] James G. Gottling, *Introduction to PSpice*, John Wiley, 1995.
[12] Ken Kundert, "Life After SPICE", *IEEE Solid-State Circuits Magazine*, Vol. 3, no. 2, 2011, pp23–26.
[13] Suhash C. Dutta Roy, "On the Realization of a Constant-Argument Immittance or Fractional Operator", *IEEE Transactions on Circuit Theory*, vol. CT-14, no. 3, September 1967, pp264–274.
[14] Ralph Morrison, "RC Constant-Argument Driving-Point Admittances", *IRE Transactions on Circuit Theory*, September 1959, pp310–317.

Jonathan Scott (M'80–SM'99) is the Foundation Professor in Electronic Engineering at the University of Waikato in Hamilton, New Zealand. From 1998 to 2006 he was with the Hewlett-Packard, now Agilent Technologies, Microwave Technology Center in Santa Rosa, where he was responsible for advanced measurement systems. In 1997 and 1998 he was Chief Engineer at RF Technology in Sydney. He was with The University of Sydney in the Department of Electrical Engineering prior to 1997. He is a Professorial Fellow of Macquarie University. Professor Scott has authored over 100 refereed publications and holds a number of patents.

Peter Single is the Principal Systems Engineer in the Implant Systems group of National Information and Communications Technology Australia. He graduated with an Electrical Engineering (Hons) degree from The University of Sydney in 1978. He was in IC designer for National Semiconductor in Sunnyvale from 1980 to 1984, and Austek Microsystems Pty Ltd in Adelaide from 1985 to 1990. He was a systems engineer at Cochlear Pty Ltd from 1991 to 2002. From 2002 to 2006 he worked for G2 Microsystems Pty Ltd (Sydney).